

Comparison of the photoluminescence properties of single NV color centers in diamond nanocrystals with single fluorescent organic molecules and optimization of the photoluminescence yield of nanodiamonds

Orestis Faklaris^a, *Jacques Botsoa*^a, *Thierry Sauvage*^b, *Jean-François Roch*^a and *François Treussart*^{a*}

^a O. Faklaris, Dr. J. Botsoa, Prof. J.-F. Roch and Prof. F. Treussart

Laboratoire de Photonique Quantique et Moléculaire, École Normale Supérieure de Cachan and CNRS UMR 8537, Cachan (France)

^b Dr. T. Sauvage

Laboratoire CEMHTI (Conditions Extrêmes et Matériaux : Haute Température et Irradiation), CNRS UPR 3079, Orléans (France)

[*] corresponding author: F. Treussart, francois.treussart@ens-cachan.fr

Laboratoire de Photonique Quantique et Moléculaire, Ecole Normale Supérieure de Cachan

61 avenue du Président Wilson, 94235, Cachan cedex, France

Tel. +33 (0) 1 47 40 75 55, Fax. +33 (0) 1 47 40 24 65

Abstract

Nitrogen-Vacancy (NV) color centers in diamond nanoparticles (NanoDiamonds, NDs) have a great number of applications, in particular in quantum information processing and as cellular fluorescent labels. In this work we compare the photoluminescence properties of a single NV color center embedded in a 30 nm diameter nanodiamond to that of a single organic fluorescent molecule. We then compare the photoluminescence properties of NDs prepared under different conditions in order to find the optimal parameters to achieve a high fluorescence yield. The results of this study are of interest for the applications of small and bright diamond nanoparticles in nanophotonics and biology.

Key words: diamond, color center, nanoparticle, photoluminescence, single molecule

1 Introduction

Solid-state nanoparticles hold great promises for applications in physics and biology. Nanoparticles like quantum dots [1, 2], gold nanobeads [3] or silicon beads [4] are used to label biomolecules with high specificity, to track their fate in cell culture systems and organisms or even to deliver drugs. Organic dyes and fluorophores are the most widely used fluorescent labels of biomolecules under ambient conditions, but they photobleach rapidly under continuous illumination [5], which makes difficult the quantification and long term follow-up. Semiconductor nanocrystals, or quantum dots, have a better stability and a lower photobleaching yield. They also offer the possibility of multicolor staining by size tuning [2]. However, the drawbacks of such nanoparticles are their potential cytotoxicity on long term scale due to their core chemical composition (cadmium and selenium) [6, 7] and their photoluminescence intermittency (photoblinking) which again makes difficult an efficient tracking of individual nanoparticles [8].

In contrast, photoluminescent nanodiamonds (PNDs) appear as promising alternative biolabels. Their photoluminescence results from embedded nitrogen-vacancy (NV) color centers in the diamond matrix [9] which present a perfect photostability with no photobleaching nor photoblinking. Moreover, it has been shown that such PNDs easily penetrate cultured cells [10, 11]. Thanks to their remarkable photoluminescence properties a reliable single particle tracking in living cells is possible [12, 13]. Other applications of NDs concern biomolecules targetted delivery which requires a control of their surface chemical groups. Grafting their surface by various bioactive moieties is a very active research field [14–16].

Additionally, NDs produced by different synthesis techniques (High Pressure and High Temperature or explosion of detonating compounds) have shown a low cytotoxicity [11, 17–19]. Considering also that PNDs can be produced in mass at tiny sizes [12, 20], a broad variety of applications can be envisioned in biology, like using them as selective labels of cellular compartments (for example mitochondria [21]) and as long term traceable delivery vehicles for biomolecules translo-

cation in cell [15, 16, 22]. Finally, the use of other types of color centers embedded in the diamond matrix can allow multi-color labeling [23].

In the field of quantum information processing, the NV color center photostability allowed to build a reliable single photon source that was used for quantum key distribution [24, 25]. Moreover numerous applications recently emerged that uses the spin unity of the NV– center. The possibility to detect the spin state of the NV center optically (via the photoluminescence intensity) facilitates the use of the NV center as a spin qubit [26] and/or its coupling with nearby electron and nuclear spins [27]. Moreover, nanodiamonds dopped with NV centers can be used as magnetic field sensors reaching atomic spatial resolution and high sensitivity [28].

The creation of small size nanodiamonds with a larger number of NV centers for applications in both biology and nanophotonics appears as a new challenge, which requires a better knowledge and control of the process that makes diamond nanoparticles photoluminescent. In the present work, we carried out a detailed quantitative comparison of the photoluminescent properties of single dye molecules and single NV color centers in nanodiamonds, confirming the perfect photostability of the color centers at only a small expense of a decrease in the fluorescence intensity compared to the one of a single molecule. To further improve the NV photoluminescence yield, we optimized the irradiation parameters allowing an increase of the NV concentration per nanodiamond.

2 Materials and methods

2.1 Production of Photoluminescent Nanodiamonds and surface functionalization

The starting material is synthetic type Ib diamond powder (SYP 0-0.05, Van Moppes, Geneva) with a specified size smaller than 50 nm. NDs are rendered photoluminescent following the procedure described in Ref. [29]. Briefly, the creation and stabilization of NV centers are performed by proton irradiation and subsequent annealing (800°C under vacuum for 2 hours). Deagglomeration of PNDs is achieved by strong acid treatment. This treatment allows us to obtain a stable colloidal suspension of NDs in deionized water. The ζ -potential of this suspension is -41.3 mV (Zetasizer Nano ZS, Malvern), and repulsive electrostatic interactions between charged surface chemical groups, mainly carboxylic [17], is probably the reason of the good stability.

We then select by centrifugation a fraction of the smallest PNDs, and measured their size distribution both in solution and after deposition on a substrate. Dynamic light scattering measurement done on the solution (apparatus: *BI-200M*, Brookhaven Instruments Corp., USA) yields an hydrodynamic diameter of 35 ± 8 nm. The heights of NDs deposited on a glass coverslip were measured by Atomic Force Microscopy (AFM, apparatus: *Nanoscope IIIa*, Veeco Instruments Inc., USA). Figure 1(a) displays a typical AFM scan of the sample, from which a mean particle height of 22 ± 8 nm was obtained and a median at 23 nm. The discrepancy between the AFM and the DLS measurements is due to the fact that PNDs have angular shapes as it can be seen on the Transmission Electron Microscopy image of Figure 1(b) (apparatus: *Tecnai F20*, operating at 200 keV). DLS measurements yields the hydrodynamic radius, considering the particles spherical, but this is not the case for this type of PNDs. Therefore, in the following of this article, we will refer to the particle studied as 30 nm in size nanodiamonds.

2.2 Study of the single-emitter photoluminescence

The optical setup used to study the photoluminescence of the single-emitter, either the single molecule or the single NV color center in a ND, is similar to the one used in Ref.[13], and is depicted on Figure 2.

The home-built confocal microscope relies on a Nikon TE300 stand, equipped with a closed loop piezoelectric three-axis scanner stage (*Tritor 102*, Piezोजना, Germany). After its reflection on the dichroic mirror DM (*530DCLP*, Chroma Corp., USA), the excitation laser beam (cw 532 nm) is focused by an oil immersion objective (Nikon Apochroma, $\times 60$, numerical aperture 1.4) onto the sample, forming a spot of area $\approx 0.6 \mu\text{m}^2$ in the focal plane. The fluorescence is then collected by the same objective. The residual excitation laser light is removed with the high-pass filter (HPF) having a transmission of 97% between 539-1200 nm (*RazorEdge LP03-532RU-25*, Semrock, USA) and an optical density of 7 at 532 nm excitation wavelength (Figure 3).

The photoluminescence spectrum is acquired with an imaging spectrograph (beam intercepted with a flip-flop Mirror (ffM)), simply relying on a concave grating (30% maximum efficiency in its first diffraction order) coupled to a cooled CCD array (back-illuminated array *DU-420-BV*, Andor Technology, Ireland).

The Hanbury Brown and Twiss time-intensity correlation setup is used to determine the number of colour centres per nanoparticle [11]. It consists of two avalanche photodiodes (APD; *SPCM-AQR14*, Perkin-Elmer, Canada) in the single-photon counting mode, on both side of a non-polarizing 50/50 beam-splitter (BS), connected to a time-correlation electronics: a Time to Amplitude Converter (*Ortec Model 566*, Ametek Inc., USA) with its output linked to a multi-channel analyzer (*Ortec 926-M32-USB*, Ametek Inc., USA) [30, 31].

The excitation laser beam is circularly polarized so that its absorption efficiency does not depend on the sample-in plane dipole orientation, which could have led to some artifact.

We evaluated the relative photoluminescence yield of single NV center compared to carbocyanine DiI_{C18} (Fluka; Spectrum Info, CAS No 41085-99-8) and Nile Red doped 20 nm diameter polystyrene beads (Invitrogen, USA). These specific dyes were chosen because their excitation spectrum is close to that of the NV color centers. Samples were prepared by spin coating on glass coverslips of a polymethyl methacrylate solution (PMMA - 1% weight, in anisol) containing dye molecules or beads, or a polyvinyl alcohol solution (PVA - 1% weight) containing PNDs, in both cases at nanomolar concentrations.

3 Results and discussion

3.1 Photoluminescence study of single dye molecules and single NV centers in PNDs

Organic dye molecules are routinely used to label biomolecules [32], but PNDs appear nowadays as promising alternative biolabels. We thus compared the photoluminescence properties of a single 30 nm PND containing a single NV center with that of a single dye molecule of carbocyanine DiI_{C18} [33]. Cyanine dyes are often used in biology as biomolecule labels for a variety of applications such as DNA sequencing or to study single molecule dynamics [34, 35].

The photoluminescence emission peak of DiI_{C18} dye is centered on 580 nm, in the range of the NV center emission spectrum. To compare the dyes to PNDs photoluminescence, we measured the signal dependence with the laser excitation intensity. This task is not easy, because most dyes photobleach rapidly under laser beam exposure of a few kW/cm² excitation intensity. In addition, detection efficiency varies and depends on the environment and the molecule dipole orientation [36, 37], which are parameters that we cannot control.

Figure 4a displays a confocal raster scan of a sample of single molecules deposited on a microscope

coverslip. We measured the counting rate as a function of the excitation laser intensity for 4 molecules and for up to ~ 14 kW/cm² excitation intensity before photobleaching (Figure 4b). The sudden diminution of the fluorescence intensity to the background level after some seconds of continuous excitation is the result of photobleaching and is a strong indication of the unicity of the examined dye molecule (Figure 4c). In order to fit the experimental data, (Figure 4b) we consider a three energy levels model. For a slow intersystem crossing rate, such a model gives a fluorescence emission rate R :

$$R(I_{\text{exc}}) = \eta_Q \times \eta_{\text{det}} \frac{k_{21}}{(k_{21}/k_{12}) + (k_{23}/k_{31}) + 1} \quad (1)$$

where η_Q is the quantum yield of the molecule, η_{det} is the overall detection efficiency, and k_{ij} the corresponding transition rates between state i and j ($i, j = 1, 2$ or 3 , corresponding respectively to the ground, the excited, and the triplet states) [38, 39]. The absorption rate k_{12} is given by the relation $k_{12} = \sigma I_{\text{exc}}/h\nu_{\text{exc}}$, where σ is the absorption cross-section of the molecule ($\sigma \approx 4 \times 10^{-16}$ cm² for the cyanine dye [40]). To get a good agreement between the model and the data, we need to take into account a dependency of k_{31} on I_{exc} of the form $k_{31} = k_{31}^0(1 + \beta I_{\text{exc}})$, which is interpreted as the pumping to higher-energy triplet states from the lower triplet state. Our data are well fitted, with $\beta = 8 \times 10^{-5}$ cm²/W, $\eta_Q \times \eta_{\text{det}} = 0.013$ and $k_{21} = 0.38$ ns⁻¹ corresponding to a radiative lifetime of 2.6 ns in good agreement with previous measurement [41].

If we consider excitation laser intensities values higher than the ones we used in the experiments where we are limited by photobleaching, and if we extend the fit of the data by equation (1) to these higher values, we obtain the saturation curve displayed in the inset of Figure 4b. We then define a saturating counting rate $R^{\text{sat}} \equiv \frac{1}{2} \times \lim_{I_{\text{exc}} \rightarrow \infty} R(I_{\text{exc}})$ which can be calculated from equation (1) with $\eta_Q \eta_{\text{det}} = 0.013$ and $k_{21} = 0.38$ ns⁻¹, yielding $R^{\text{sat}}(\text{cy}) = 2475$ kcounts/s. The corresponding saturation excitation intensity associated to this counting rate is $I_{\text{exc}}^{\text{sat}}(\text{cy}) = 1700$ kW/cm². This counting rate at saturation value is relatively high, but it is never reached

due to photobleaching. Just before photobleaching, the counting rate of a single molecule is ~ 80 kcounts/s.

To study a system brighter than single organic molecules, we examined a sample of 20 nm beads doped with Nile Red (Invitrogen, USA), frequently used as labels. Figure 4d shows the time trace of the fluorescence intensity of one fluorescent bead under 532 nm cw excitation. We clearly see a stronger fluorescence signal than the one of a single DilC_{18} molecule. However, after 20 seconds of illumination this signal almost vanishes due to photobleaching. The diminution of fluorescence occurs by steps, indicating the gradual photobleaching of the molecules one by one.

We then examined 30 nm diameter PNDs. Figure 5a shows a confocal raster scan, where we observe many photoluminescence spots with different intensities, due to an inhomogeneous number of NV centers per nanocrystal. On the left side of some spots is indicated the number of NV centers embedded in the corresponding PNDs. This amount was determined with photon intensity-time correlation measurements. For a simple two-level quantum system, which can emit only one photon at a time (the so-called photon-antibunching), the probability of emitting two consecutive photons gradually drops to zero as the time-lag between them decreases. This results in a dip at the zero time delay of the normalized second order time-intensity correlation function. When we excite the fluorescence of n emitters, the latter function displays a smaller dip of depth $1/n$ allowing the determination of the number n of emitters [42] (see Figure 5d).

With the help of such measurements we were able to select nanocrystals containing a single NV center (Figure 5b) and to record its photoluminescence intensity saturation curve. As emission rates depend on the environment of the NV center and the NV dipole orientation, we recorded the saturation curve for 3 single NV centers (marked with arrows on the scan) and then calculated the mean value (in blue) (Figure 5e). The photoluminescence spectra of the studied PNDs correspond either to the emission of the neutral NV° (with no electric charge) or the negatively charged NV^{-} (Figure 5c) color center, identified thanks to their Zero Phonon Line (ZPL) at 575 nm and 637 nm respectively.

The laser excitation power at saturation for the mean curve is $P^{\text{sat}}(\text{NV}) = 0.44$ mW, which corresponds to an intensity of $I_{\text{exc}}^{\text{sat}}(\text{NV}) = 530$ kW/cm². This latter value is found by fitting the experimental data with the function $R(I_{\text{exc}}) = \frac{2R^{\text{sat}}}{1 + I_{\text{exc}}^{\text{sat}}/I_{\text{exc}}}$, yielding at the same time $R^{\text{sat}} = 31$ kcounts/s.

We summarize in Table 1 the photophysical properties of the carbocyanine and the NV center as calculated from the experimental data fitted with appropriate functions. The saturation excitation intensity ratio calculated from fitted data is $I_{\text{exc}}^{\text{sat}}(\text{cy})/I_{\text{exc}}^{\text{sat}}(\text{NV}) \approx 3.2$. This result can be explained by the differences in the absorption cross sections σ and in the emitter radiative lifetimes τ_{rad} of the two systems, because $I_{\text{exc}}^{\text{sat}}$ is roughly proportional to $(\sigma\tau_{\text{rad}})^{-1}$. Putting the different values indicated in Table 1 together, one gets $[\sigma(\text{NV})\tau_{\text{rad}}(\text{NV})]/[\sigma(\text{cy})\tau_{\text{rad}}(\text{cy})] \approx 2.5$, which is close to the ratio of the saturation values of excitation intensities.

3.2 Optimization of the photoluminescence yield of nanodiamonds

In contrary to single DilC₁₈ molecules or Nile Red-doped beads, we observe that the photoluminescence intensity of a single NV center is perfectly constant over time (Figure 5f). Additionally, in the case of a PND containing 4 NV centers (Figure 5d), we observe a 4-5 fold increase of the photoluminescence intensity compared to the single NV center (1152 and 299 average counts/20 ms respectively), corresponding to a signal three times higher than the one of the single cyanine molecule just before its photobleaching occurs.

The possibility to further increase the concentration of NV centers in NDs will enhance their natural photoluminescence and allow a better detection for labeling applications in biology. Active NV centers are created in nitrogen-rich ([N]~100 ppm) type Ib diamond crystal by a two steps procedure involving the generation of vacancies by electron or ion beams followed by thermal annealing of vacancy defects at temperature > 600°C. At such temperatures the vacancies start migrating to the nearest substitutional nitrogen atoms [43, 44]. The conversion efficiency can

however be limited due to competitive processes such as the formation of other defects and vacancy-interstitial recombination. We explore the possibility to improve the NV color center creation yield by increasing the number of vacancies created in the diamond matrix by high energy beam irradiation. To this purpose we varied the irradiation dose of H^+ ions applied to PNDs. Type Ib NDs were irradiated at doses of either $5 \times 10^{15} H^+/cm^2$ or $5 \times 10^{16} H^+/cm^2$ and then annealed at $800^\circ C$ for 2 h. It is worth to note that the latter dose is the highest proton irradiation dose used so far for this type of applications. After irradiation, thermal annealing, acid cleaning, re-suspension in water and size selection, the solutions of PNDs corresponding to each irradiation dose were deposited by spin coating on glass coverslips. Figure 6a,b shows the photoluminescence confocal raster scans for the two irradiation doses. Next to each spot is indicated the measured number n of NV centers. For the low proton irradiation dose we infer a mean value of $n = 2.7 \pm 1.1$ NV centers/ PND, while for the 10 times higher dose the mean value is $n = 7.0 \pm 2.1$ NV centers/ PND. Figure 6c shows a comparison of the PNDs photoluminescence intensity distribution for the two irradiation doses, with 75 and 100 nanoparticles respectively. We find a broad distribution in each case. For the low irradiation dose the median value is 315 kcounts/s while it is 986 kcounts/s for the one order of magnitude higher dose, indicating a 3 fold increase of the corresponding photoluminescence signal.

3.3 Discussion on the efficiency of NV center creation

To get a better understanding of the above results we simulated the radiation damages in the diamond lattice due to ions irradiation using the SRIM Monte Carlo simulations (software available at <http://www.srim.org/>). According to these simulations, a 2.4 MeV proton can penetrate in diamond up to a depth of $30 \mu m$ (Figure 7). Moreover, in order to create an homogeneous distribution of vacancies in all the nanodiamonds (flat region Figure 7 curve), we prepared a thin layer of these particles of thickness smaller than $30 \mu m$ on a silicon wafer. SRIM simulations predict that in this flat region the density of created vacancies is 8.17×10^{-6} vacancies/ $\text{\AA}/H^+$, i.e.

817 vacancies/cm/H⁺ (Figure 7). Considering that for proton irradiation the damage efficiency is about 10 vacancies per H⁺ ion (if the beam incident on the [111] direction, otherwise in case it is incident on the [100] direction it is 13 vacancies per proton [45]), the 5×10^{15} H⁺/cm² dose produces per unit surface 5×10^{16} vacancies/cm² while the 5×10^{16} H⁺/cm² dose produces 5×10^{17} vacancies/cm².

For a 30 nm diameter nanodiamond, the irradiation dose of 5×10^{16} H⁺/cm² is therefore expected to produce *in volume* 4×10^{20} vacancies/cm³ resulting in ~ 5600 vacancies. Taking into consideration the initial concentration of nitrogen in the type 1b of diamond used (~ 100 ppm, equivalent to 1.76×10^{19} N/cm³), we calculate that we have 480 N atoms in a 30 nm nanodiamond. Our observations therefore indicate that a large proportion of the available nitrogen and created vacancies in the nanodiamond matrix is not converted into NV centers. The estimated ratio of the mean number of NV centers created (7), measured by time intensity correlations, to the number of nitrogen atoms is about 7:480.

A way to increase the PNDs brightness once we reach the highest vacancies concentration is to improve the conversion rate of non-complexed vacancies and nitrogen atoms to NV centers. The theoretical conversion percentage of 25 - 30% [46], confirmed experimentally in recent studies [45], is not yet achieved for nanodiamonds in our experiments and is still a lot of margin for further improvement.

However, it has been recently reported that the probability of NV centers creation in nanocrystals decreases with the square of the particle radius when the particles have tiny sizes (~ 10 nm) [47]. This is a consequence of the fact that defects are stable only within the core region of the nanodiamonds, and annihilate at the surface during the thermal treatment without forming NV centers. In order to increase the number of NV centers in small size nanodiamonds, different strategies may be envisioned. The first one consists of changing the irradiation and annealing conditions. Here we used the maximal proton irradiation dose, the next step is to alter the annealing parameters. The second strategy consists in creating NV centers in bigger size diamond

crystals, which can then be reduced in size by milling. This method was applied by Curmi *et al.* [20] and they report the observation of a 10 nm nanodiamond containing 12 NV centers. The last method is by creating the NV centers in large size nanodiamonds (50-100 nm) and then reduce them in size by oxidative etching (in air at 500 °C for 1 – 2 h) [48]. An overall 7-fold increase of the photoluminescence intensity was reported in the later case. Note that in all cases, the PNDs have inhomogeneous photoluminescence intensities: some particles are very bright, while other contain only a single color center. Despite these recent progresses, the synthesis of small and homogeneously bright nanodiamonds still deserve more effort to meet the standards of commercial labels used for bioimaging.

4 Conclusion

In this work we showed that contrary to dye molecules, the emission of single NV centers in single nanodiamonds is perfectly stable in time, with similar maximal photoluminescence signals in practical conditions. In order to improve the NDs photoluminescence yield, we optimized the parameters of the proton irradiation beam used to create high concentrations of vacancies in 30 nm diameter NDs and we gained a factor of three regarding the photoluminescence intensity. After calculations we conclude that there is still plenty of room to improve the conversion of the available vacancies and nitrogen atoms in the diamond matrix into NV color centers, by proper optimization of the sample preparation conditions and adjustment of other parameters than the irradiation dose. Our results contribute to a better control of the NV color center generation in nanodiamonds, an important step towards the creation of strongly photoluminescent nanodiamonds for applications in biology and nanophotonics.

5 Acknowledgements

We thank Géraldine Dantelle for the measurements of the zeta potential of the nanodiamond colloidal suspension, Alain Thorel for the TEM image of the PNDs and Jean-Paul Boudou for the acid treatment of the nanodiamonds. This work was supported by the European Commission under the project “Nano4Drugs” (contract LSHB-2005-CT-019102), by Agence Nationale de la Recherche under the project “NaDia” (contract ANR-2007-PNANO-045) and by “Île de France” Region *C’Nano* grant under the project “Biodiam”.

References

- [1] A.P. Alivisatos. The use of nanocrystals in biological detection. *Nature Biotech.*, 22:47–52, 2004.
- [2] X. Michalet, F. Pinaud, L. Bentolila, J. Tsay, S. Doose, J.J. Li, G. Sundaresan, A.M. Wu, S. Gambhir, and S. Weiss. Quantum dots for live cells, in vivo imaging, and diagnostics. *Science*, 307:538–544, 2005.
- [3] D. Lasne, G. Blab, S. Berciaud, M. Heine, L. Groc, D. Choquet, L. Cognet, and B. Lounis. Single nanoparticle photothermal tracking (snapt) of 5-nm gold beads in live cells. *Biophys. J.*, 91:4598 – 4604, 2006.
- [4] J.H. Warner, A. Hoshino, K. Yamamoto, and R.D. Tilley. Water-soluble photoluminescent silicon quantum dots. *Angew. Chem. Int. Ed.*, 44:4550 – 4554, 2005.
- [5] U. Resch-Genger, M. Grabolle, S. Cavaliere-Jaricot, R. Nitschke, and T. Nann. Quantum dots versus organic dyes as fluorescent labels. *Nat. Methods*, 9:763–775, 2008.
- [6] C. Kirchner, T. Liedl, S. Kudera, T. Pellegrino, A. Javier, H. Gaub, S. Stoelze, N. Fertig,

- and W.J. Parak. Cytotoxicity of Colloidal CdSe and CdSe/ZnS Nanoparticles. *Nano Lett.*, 5:331, 2005.
- [7] N. Lewinski, V. Colvin, and R. Drezek. Cytotoxicity of nanoparticles. *Small*, 4:26–49, 2008.
- [8] M. Nirmal, B. Dabbousi, M.G. Bawendi, J.J. Macklin, J.K. Trautman, T.D. Harris, and L.E. Brus. Fluorescence intermittency in single cadmium selenide nanocrystal. *Nature*, 383:802–804, 1996.
- [9] A. Gruber, A. Dräbenstedt, C. Tietz, L. Fleury, J. Wrachtrup, and C. Von Borczyskowsky. Scanning confocal optical microscopy and magnetic resonance on single defect centers. *Science*, 276:2012, 1997.
- [10] S.-J. Yu, M.-W. Kang, H.-C. Chang, K.-M. Chen, and Y.-C. Yu. Bright Fluorescent Nanodiamonds: No Photobleaching and Low Cytotoxicity. *J. Am. Chem. Soc.*, 127:17604–17605, 2005.
- [11] O. Faklaris, D. Garrot, V. Joshi, F. Druon, J.P. Boudou, T. Sauvage, P. Georges, P.A. Curmi, and F. Treussart. Detection of single photoluminescent diamond nanoparticles in cells and study of their internalization pathway. *Small*, 4:2236–2239, 2008.
- [12] Y.-R. Chang, H.-Y. Lee, K. Chen, C.-C. Chang, D.-S. Tsai, C.-C. Fu, T.-S. Lim, Y.-K. Tzeng, C.-Y. Fanf, C.-C. Han, H.-C. Chang, and W. Fann. Mass production and dynamic imaging of fluorescent nanodiamonds. *Nature Nanotech.*, 3:284–288, 2008.
- [13] O. Faklaris, D. Garrot, V. Joshi, J.P. Boudou, T. Sauvage, P.A. Curmi, and F. Treussart. Comparison of the photoluminescence properties of semiconductor quantum dots and non-blinking diamond nanoparticles and observation of the diffusion of diamond nanoparticles in living cells. *J. Europ. Opt. Soc. Rap. Public.*, 4:09035, 2009.
- [14] A. Krüger. Diamond nanoparticles for biological applications. *J. Chem. Eur.*, 14:1382, 2008.
- [15] J.-I. Chao, E. Perevedentseva, P.-H. Chung, K.-K. Liu, C.-Y. Cheng, C.-C. Chang, and

- C.-L. Cheng. Nanometer-sized diamond particle as a probe for biolabeling. *Biophys. J.*, 93:2199–2208, 2007.
- [16] S. Vial, C. Mansuy, S. Sagan, T. Irinopoulou, F. Burlina, J.P. Boudou, G. Chassaing, and S. Lavielle. Peptide-grafted nanodiamonds: preparation, cytotoxicity and uptake in cells. *ChemBioChem*, 9:2113–2119, 2008.
- [17] C.-C. Fu, H.-Y. Lee, K. Chen, T.-S. Lim, H.-Y. Wu, P.-K. Lin, P.-K. Wei, P.-H. Tsao, H.-C. Chang, and W. Fann. Characterization and applications of single fluorescent nanodiamonds as cellular biomarkers. *Proc. Natl. Acad. Sc. USA*, 104:727, 2007.
- [18] A. M. Schrand, H. Huang, C. Carlson, J. Schlager, E. Osawa, S.M. Hussain, and L. Dai. Are diamond nanoparticles cytotoxic? *J. Phys. Chem. B*, 111(1):2–7, 2007.
- [19] K.K. Liu, C.L. Cheng, and C.C. Chang. Biocompatible and detectable carboxylated nanodiamond on human cell. *Nanotechnology*, 18:325102, 2007.
- [20] J.P. Boudou, P.A. Curmi, F. Jelezko, J. Wrachtrup, P. Aubert, M. Sennour, G. Balasubramanian, R. Reuter, A. Thorel, and E. Gaffet. High yield fabrication of fluorescent nanodiamonds. *Nanotechnology*, 20:235602, 2009.
- [21] M. Mkandawire, A. Pohl, T. Gubarevich, V. Lapina, D. Appelhans, G. Rödel, W. Pompe, J. Schreiber, and J. Opitz. Selective targeting of green fluorescent nanodiamond conjugates to mitochondria in HeLa cells. *J. Biophot.*, 2:596–606, 2009.
- [22] H. Huang, E. Pierstorff, E. Osawa, and D. Ho. Active nanodiamond hydrogels for chemotherapeutic delivery. *Nano Lett.*, 7(11):3305–3314, NOV 2007.
- [23] T.-L. Wee, Y.-W. Mau, C.-Y. Fang, H.-L. Hsu, C.-C. Han, and H.-C. Chang. Preparation and characterization of green fluorescent nanodiamonds for biological applications. *Diamond Relat. Mater.*, 18:567–573, 2009.

- [24] A. Beveratos, R. Brouri, T. Gacoin, A. Villing, J.-P. Poizat, and P. Grangier. Single photon quantum cryptography. *Phys. Rev. Lett.*, 89:187901, 2002.
- [25] R. Alléaume, F. Treussart, G. Messin, J.-F. Roch, Y. Dumeige, A. Beveratos, R. Brouri, J.-P. Poizat, and P. Grangier. Experimental open-air quantum key distribution with a single photon source. *New J. Phys.*, 6:92, 2004.
- [26] F. Jelezko, T. Gaebel, I. Popa M. Dohman, A. Gruber, and J. Wrachtrup. Observation of coherent oscillations of a single nuclear spin and realization of a two-qubit conditional quantum gate. *Phys. Rev. Lett.*, 93:130501, 2004.
- [27] T. Gaebel, M. Domhan, I. Popa, C. Wittmann, P. Neumann, F. Jelezko, J.R. Rabeau, N. Stavrias, A.D. Greentree, S. Prawer, J. Meijer, J. Twamley, P.R. Hemmer, and J. Wrachtrup. Room-temperature coherent coupling of single spins in diamond. *Nat. Physics*, 2:408–413, 2006.
- [28] G. Balasubramanian, I.Y. Chan, R. Kolesov, M. Al-Hmoud, J. Tisler, C. Shin, C. Kim, A. Wojcik, P.R. Hemmer, A. Krueger, T. Hanke, A. Leitenstorfer, R. Bratschitsch, F. Jelezko, and J. Wrachtrup. Nanoscale imaging magnetometry with diamond spins under ambient conditions. *Nature*, 455:648–651, 2008.
- [29] Y. Sonnefraud, A. Cuche, O. Faklaris, J.-P. Boudou, T. Sauvage, J.-F. Roch, F. Treussart, and S. Huant. Diamond nanocrystals hosting single NV color centers sorted by photon-correlation near-field microscopy. *Opt. Lett.*, 33:611, 2008.
- [30] F. Treussart, V. Jacques, E Wu, T. Gacoin, P. Grangier, and J.-F. Roch. Photoluminescence of single colour defects in 50 nm diamond nanocrystals. *Physica B*, 376:926–929, 2006.
- [31] A. Beveratos, R. Brouri, T. Gacoin, J.-Ph. Poizat, and Ph. Grangier. Nonclassical radiation from diamond nanocrystals. *Phys. Rev. A*, 64:061802, 2001.
- [32] S. Weiss. Fluorescence spectroscopy of single biomolecules. *Science*, 283:1676, 1999.

- [33] F. Treussart, R. Alléaume, V. Le Floch, L.T. Xiao, J.-M. Courty, and J.-F. Roch. Direct measurement of the photon statistics of a triggered single photon source. *Phys. Rev. Lett.*, 89:093601, 2002.
- [34] S.C. Blanchard, H.D. Kim, R.L. Gonzalez, J.D. Puglisi, and S. Chu. tRNA dynamics on the ribosome during translation. *Proc. Natl. Acad. Sci. USA*, 101:12893–12898, 2004.
- [35] L.S. Churchman, Z. Okten, R.S. Rock, J.F. Dawson, and J.A. Spudich. Single molecule high-resolution colocalization of Cy3 and Cy5 attached to macromolecules measures intramolecular distances through time. *Proc. Natl. Acad. Sci. USA*, 102:1419–1423, 2005.
- [36] E.M. Purcell. Spontaneous emission probabilities at radio frequencies. *Phys. Rev. B*, 69:681, 1946.
- [37] K. H. Tews, O. Inacker, and H. Kuhn. Variation of the Luminescence Lifetime of a Molecule Near an Interface Between Different Polarizable Dielectrics - Erratum. *Nature*, 228:791, 1970.
- [38] F. Treussart, A. Clouqueur, C. Grossman, and J.-F. Roch. Photon antibunching in the fluorescence of a single dye molecule embedded in a thin polymer film. *Opt. Lett.*, 26:1504, 2001.
- [39] T. Basche, W.E. Moerner, M. Orrit, and U.P. Wild. *Single-Molecule Optical Detection, Imaging and Spectroscopy*. VCH, Weinheim, Germany, 1st edition, 1997.
- [40] H. Gruber, C. Hahn, G. Kada, C. Riener, G. Harms, W. Ahrer, T. Dax, and H.G. Knaus. Anomalous Fluorescence Enhancement of Cy3 and Cy3.5 versus Anomalous Fluorescence Loss of Cy5 and Cy7 upon Covalent Linking to IgG and Noncovalent Binding to Avidin. *Bioconj. Chem.*, 5:696–704, 2000.
- [41] F. Treussart, R. Alléaume, V. Le Floch, and J.F. Roch. Single photon emission from a single molecule. *C. R. Physique*, 3:501–508, 2002.

- [42] G. Greenstein and A.G. Zajonc. *The Quantum Challenge*. Jones and Bartlett, 2nd edition, 2005.
- [43] L. Allers, A.T. Collins, and J. Hiscock. The annealing of interstitial-related optical centres in type II natural and CVD diamond. *Diamond Relat. Mater.*, 7:228–232, 1998.
- [44] N.B. Iakoubovskii and G.J. Adrianenssens. Trapping of vacancies by defects in diamond. *J. Phys. C*, 13:6015–6018, 2001.
- [45] T.-S. Wee, Y.-K. Tzeng, C.-C. Han, H.-C. Chang, W. Fann, J.-H. Hsu, K.-M. Chen, and Y.-C. Yu. Two-photon Excited Fluorescence of Nitrogen-Vacancy Centers in Proton-Irradiated Type Ib Diamond. *J. Phys. Chem. A*, 111:9379–9386, 2007.
- [46] S.C. Lawson, D. Fisher, D. Hunt, and M. Newton. On the existence of positively charged single- substitutional nitrogen in diamond. *J. Phys. Condens. Matter*, 10:6171–6180, 1998.
- [47] A. V. Zvyagin, D. Gruber, C. J. Noble, R. Vogel, E. Sawa, and T. Plakhotnik. Five-Nanometer Diamond with Luminescent Nitrogen-Vacancy Defect Centers. *Small*, 14:1591–1595, 2009.
- [48] N. Mohan, Y.-K. Tzeng, L. Yang, Y.-Y. Chen, Y.Y. Hui, C.-Y. Fang, and H.-C. Chang. Sub-20-nm fluorescent nanodiamonds as photostable biolabels and fluorescence resonance energy transfer donors. *Adv. Mater.*, 10.1002/adma.200901596, 2009.
- [49] J. Tisler, G. Balasubramanian, B. Naydenov, R. Kolesov, B. Grotz, R. Reuter, J.-P. Boudou, P. A. Curmi, M. Sennour, A. Thorel, M. Boersch, K. Aulenbacher, R. Erdmann, P.R. Hemmer, F. Jelezko, and J. Wrachtrup. Fluorescence and Spin Properties of Defects in Single Digit Nanodiamonds. *ACS Nano*, 3:1959–1965, 2009.

Tables

	$\sigma \times 10^{-17} \text{ cm}^2$	τ_{rad} (ns)	$I_{\text{exc}}^{\text{sat}}$ (kW/cm ²)	R^{sat} (kcounts/ s)
single carbocyanine molecule	40-60 ^a	2.6 ^b	1700 ⁱ 14.5 ⁱⁱ	2475 ⁱ 74 ⁱⁱ
single NV in PND	3 ^c	17 ± 15 ^d	529 ± 70	31

Table 1: Comparison of the photophysical properties of single molecules and single NV centers in PNDs. Excitation laser at 532 nm. For single carbocyanine molecules, i) are the values obtained by extrapolation of the 3-levels fit, ii) are the measured maximal values before photobleaching occurs. References: a: [40], b: [41], c: [45], d: [49]

Figure Captions

Figure 1: Size distribution and shape of the PNDs used in this study: a) AFM scan of PNDs spincoated on a glass coverslip; b) TEM image showing PNDs angular shape; c) distribution of heights of the nanodiamonds observed in AFM scan (a). Mean value: 22 ± 8 nm. Number of particles analyzed: 73.

Figure 2: Optical setup used to study PNDs photoluminescence. Surrounded by the blue dashed-line box: the home-built confocal microscope. The Hanbury Brown and Twiss time correlation system is depicted in the black dashed-line box. We modified the commercial microscope in order to get a collimated beam at its output port. This modification consists in the addition of a diverging lens DL (focal length: -125 mm) after the lens tube turning the beam back into a collimated one, easier to handle for further propagation. The collimated output beam is then focused by the L1 lens (100 mm focal length) into the 50 μm pinhole (PH).

Figure 3: Absorption (in green) and emission (in red) spectra of carbocyanine DiIC₁₈(3) molecules. The vertical black line shows the 532 nm excitation laser. The blue dashed line is the long-pass (RazorEdge LP03-532RU-25) filter transmittance and the purple dashed line is the dichroic 530DCLP transmittance. Note that the choice of these filters is optimal for the carbocyanine

fluorescence spectrum.

Figure 4: Photoluminescence of single dye molecules : a) Confocal raster scan, cw excitation laser at 532 nm, intensity 12 kW/cm^2 (power $20 \text{ }\mu\text{W}$); b) Counting rate versus excitation intensity for 4 molecules (dashed colored); the plain line in green is the fit according to the three-level model expression of equation (1). Inset: the saturation curve for higher excitation intensity values; c) A 20 s intensity time-trace of a single molecule (binning 20 ms) with the characteristic one-step bleaching, cw excitation laser at 532 nm, intensity 6 kW/cm^2 ; d) Time-trace for a 20 nm Nile Red-doped polystyrene bead, excitation 24 kW/cm^2 .

Figure 5: Photoluminescence study of single NV centers in single PNDs: a) Confocal raster scan of 30 nm PNDs deposited on a glass coverslip by spin-coating. Excitation cw laser at 532 nm, intensity 0.6 MW/cm^2 (power 1 mW); the image scale is saturated at 3000 counts/20 ms, in order to see easier the less intense spots; the numbers on the left of the spots correspond to the number of NV centers per particle; b) Intensity time correlation function of the PND in red square, showing photon antibunching at zero delay, proving that the studied color center is single; c) Photoluminescence spectrum of the same PND, corresponding to the emission of NV^- color center; d) Intensity time correlation function of the PND with blue (vertical) arrow of the scan a). From the antibunching dip we infer $n = 4$ NV centers; e) Counting rate versus excitation intensity for 3 single NV centers (dashed colored), with plain green the saturation fitting curve; f) Time monitoring of the photoluminescence intensity of a single NV center and a ND containing 4 NV centers (of (b) and (d) respectively) over a period of 600 s, showing the perfect photostability (binning 20 ms).

Figure 6: Photoluminescence comparison of 30 nm PNDs spin-coated on glass coverslips, after H^+ irradiation and annealing. The well isolated spots correspond to single PNDs, with the numbers next to each spot illustrating the number n of NV centers per PND. a) Confocal scan of PNDs irradiated with $5 \times 10^{15} \text{ p}^+/\text{cm}^2$, mean value $n = 2.7 \pm 1.1$ NV centers/ PND ; b) Confocal scan of PNDs irradiated with $5 \times 10^{16} \text{ p}^+/\text{cm}^2$, mean value $n = 7 \pm 2.1$ NV centers/ PND ; exc.

wavelength 532 nm, exc. power 1 mW ; c) Occurrence versus photoluminescence intensity for NDs irradiated with $5 \times 10^{15} \text{ H}^+/\text{cm}^2$ (in blue) and $5 \times 10^{16} \text{ H}^+/\text{cm}^2$ (in red) respectively.

Figure 7: Spatial distribution of vacancies produced in diamond by ion beam irradiation as predicted by SRIM Monte Carlo simulations for 2.4 MeV proton irradiation. The numbers of damage events used in the simulations were 9999.

Figures

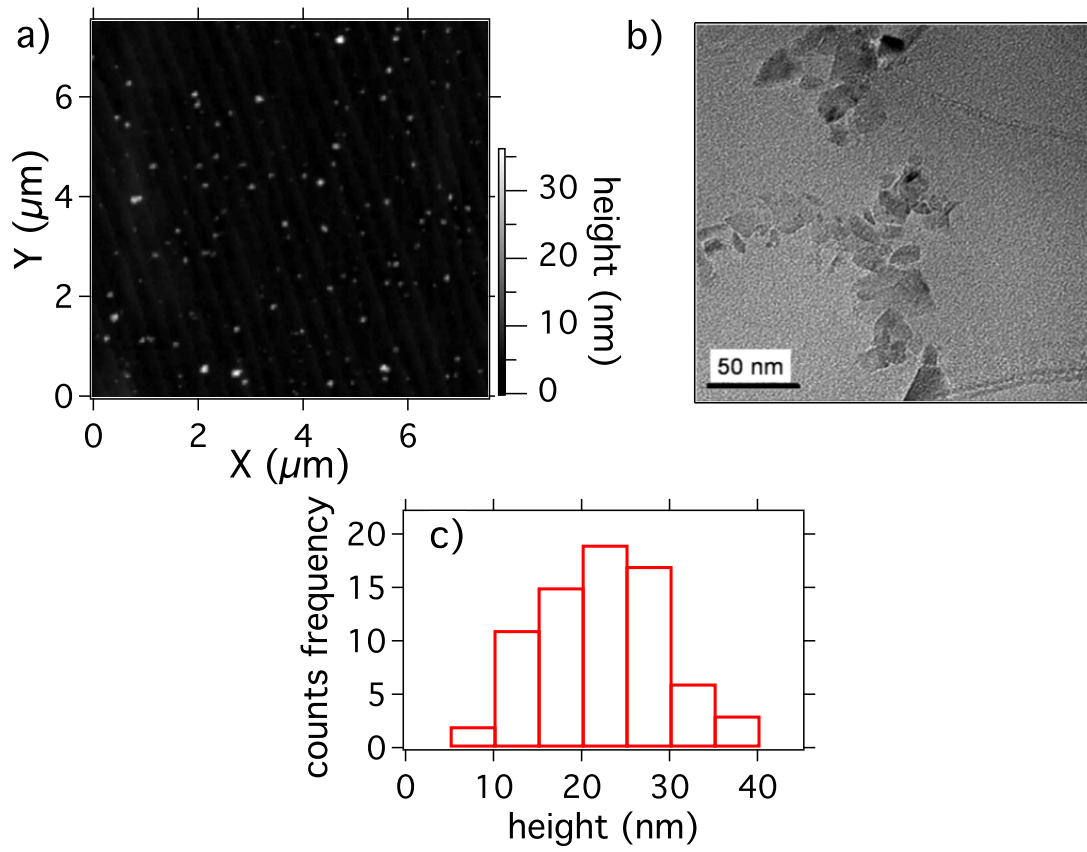


Figure 1:

Home-built confocal microscope

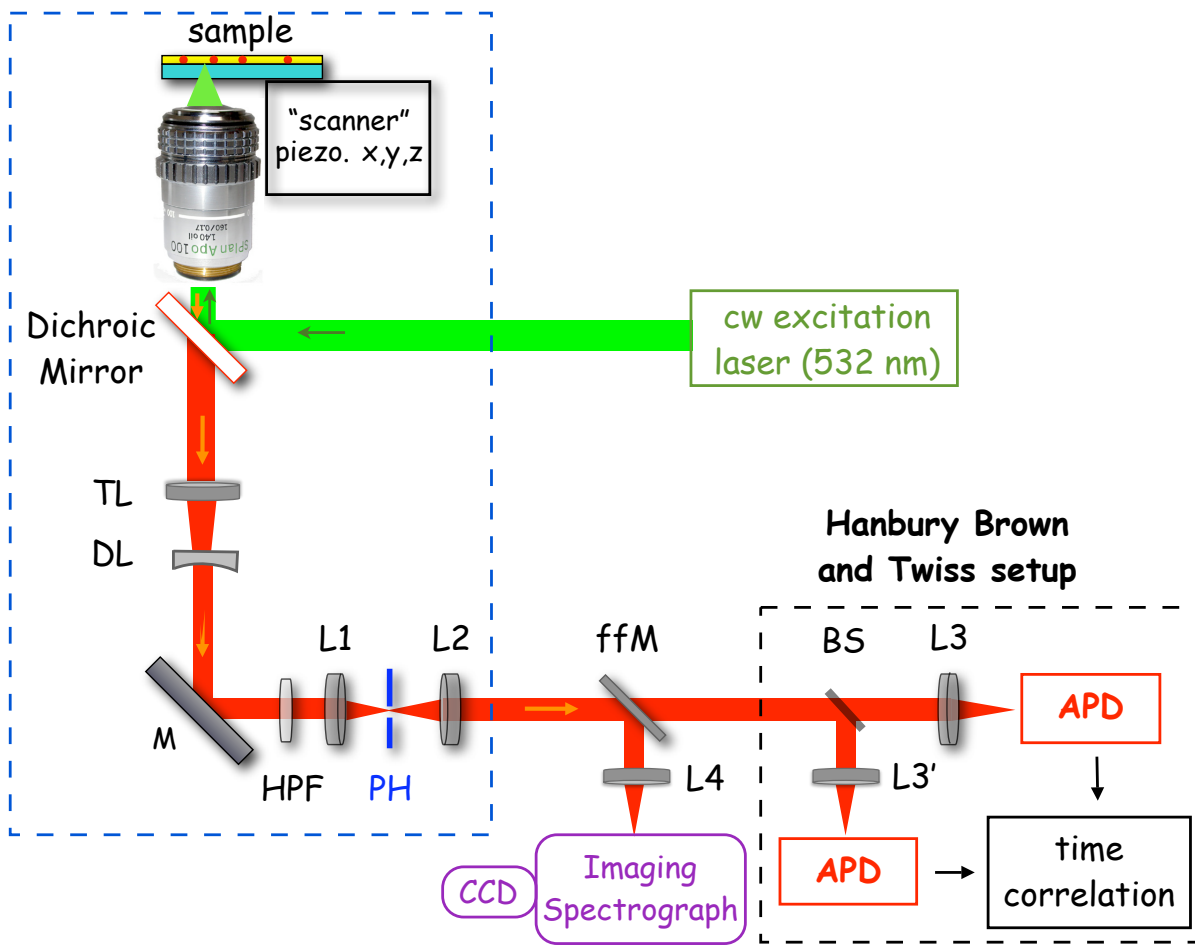


Figure 2:

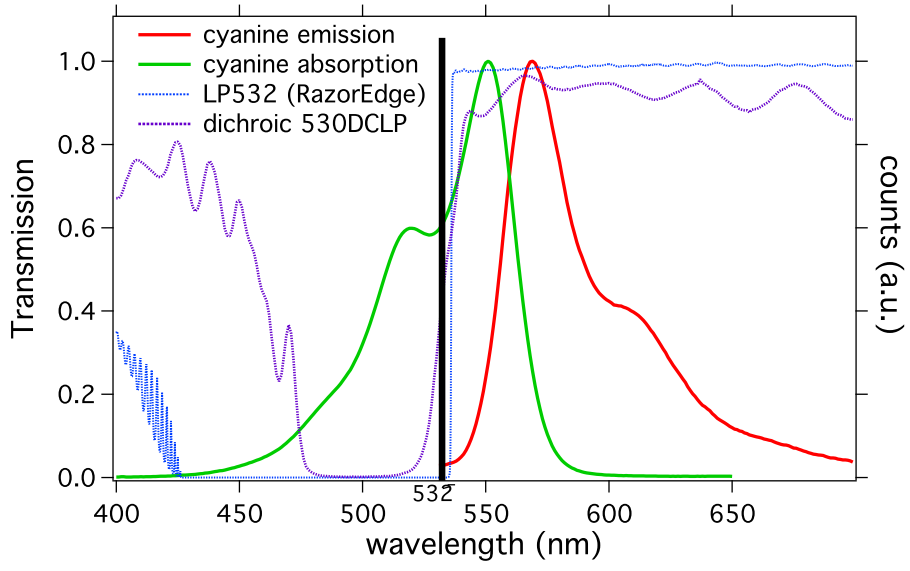


Figure 3:

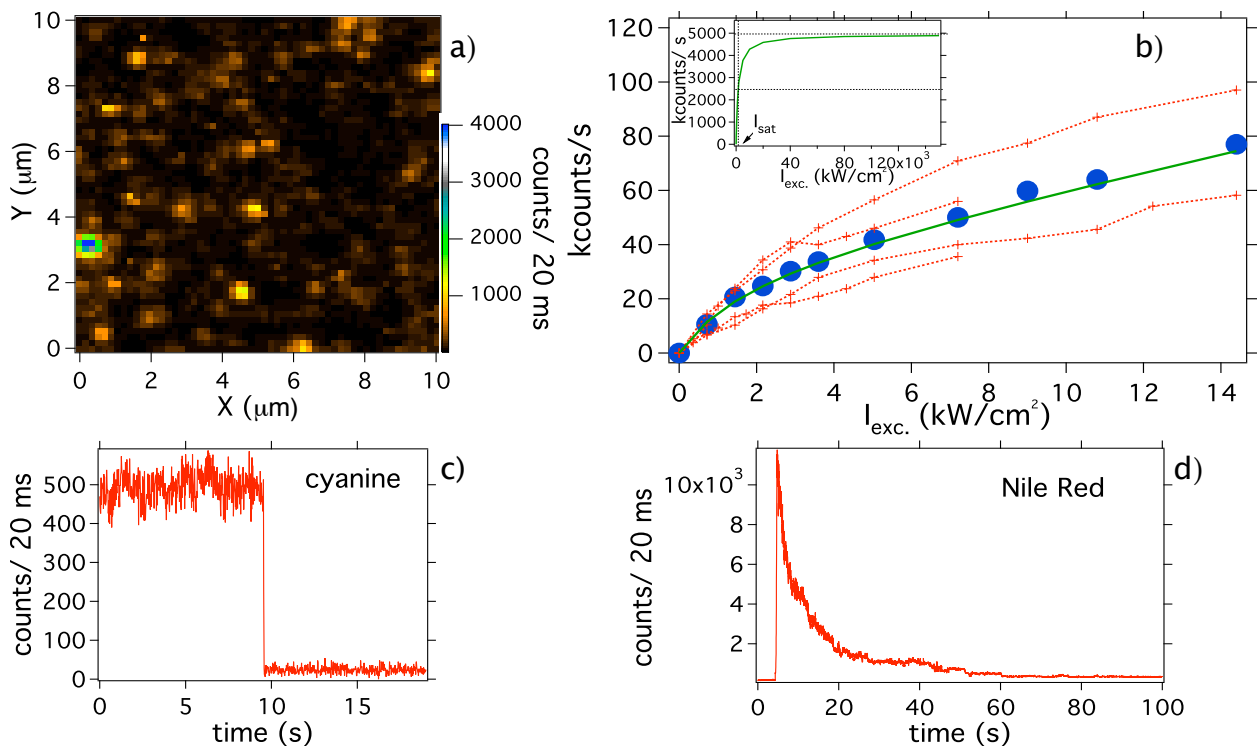


Figure 4:

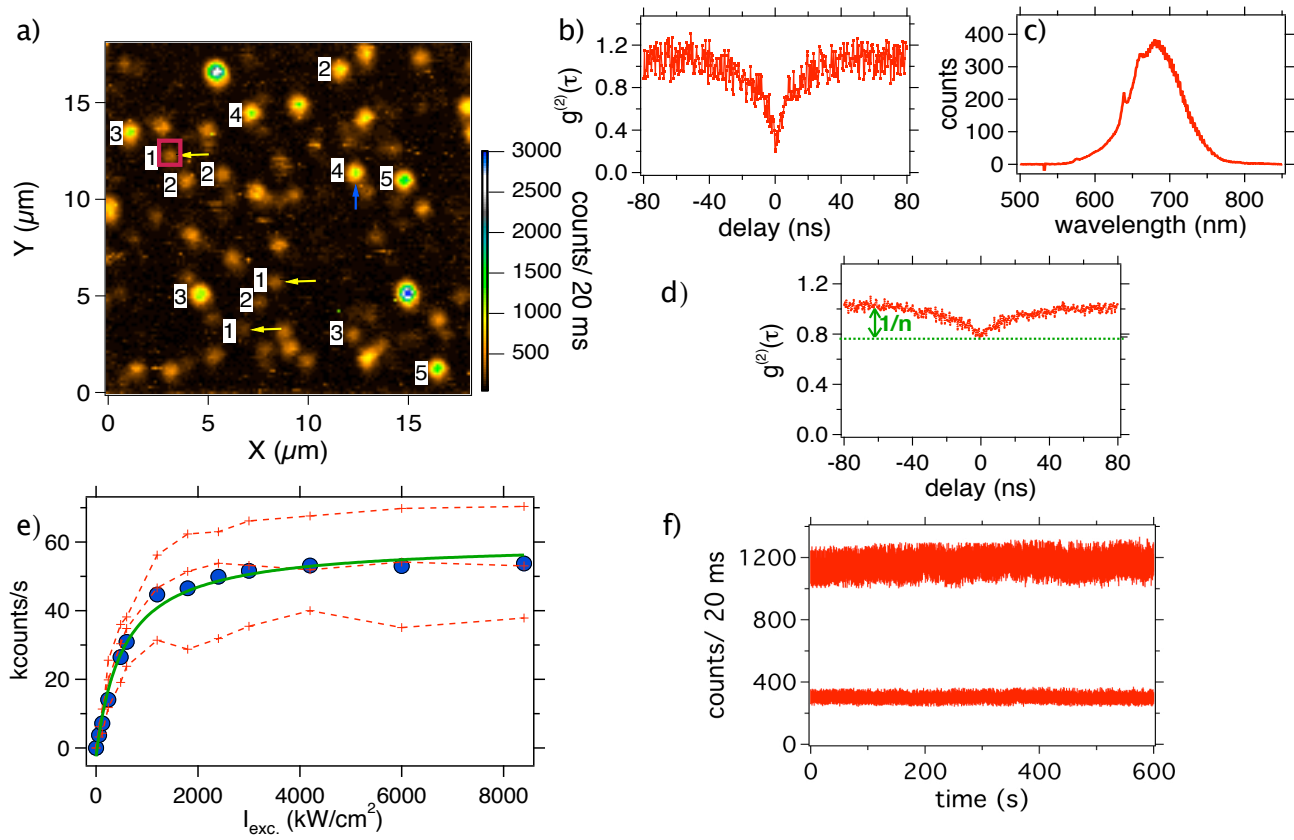


Figure 5:

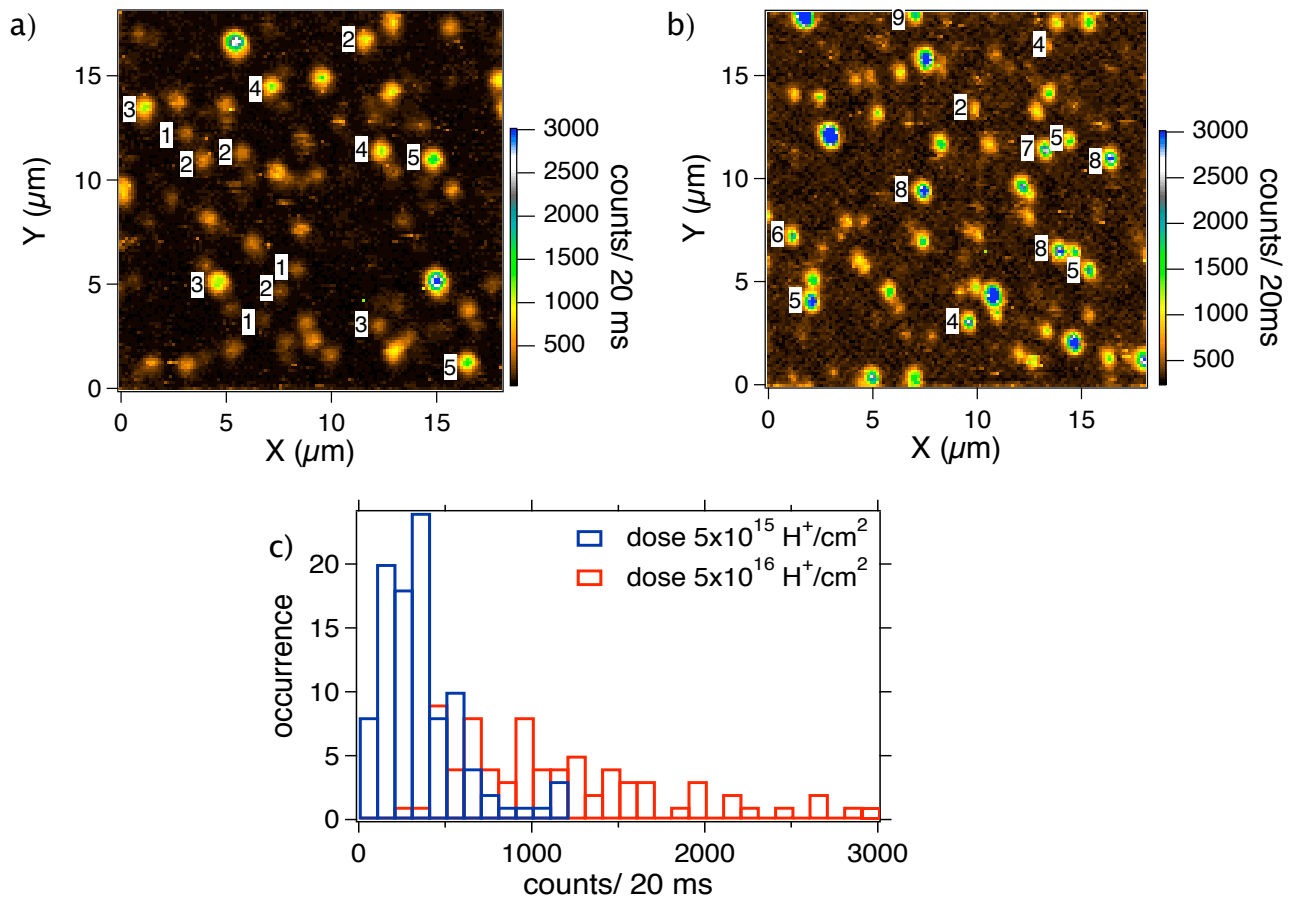


Figure 6:

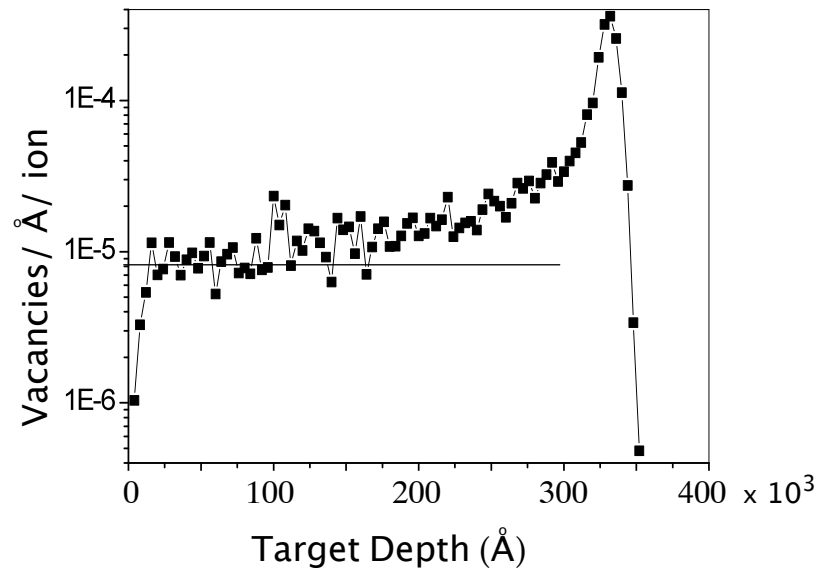


Figure 7: